THE EFFECT OF SCHMIDT NUMBER ON THE MIXING IN THE WALL REGION OF AN IMPINGING JET

Johan Revstedt
Div. of Fluid Mechanics, Lund Institute of Technology
SE-221 00 Lund, Sweden
Johan.Revstedt@vok.lth.se

Laszlo Fuchs
Div. of Fluid Mechanics, Lund Institute of Technology
SE-221 00 Lund, Sweden
Laszlo.Fuchs@vok.lth.se

ABSTRACT

Large Eddy Simulation of a semi-confined impinging jet at Reynolds number 10000 was performed. The impingement distance was varied between 2 and 6 nozzle diameters. The unsteady spatially filtered incompressible Navier-Stokes equations were solved together with a transport equation for the concentration of an inert additive using a multi-grid finite difference code with a staggered grid. The un-resolved scales of the flow as well as the sub-grid scale mixing were modelled implicitly through the truncation errors of the discretisation. The transport of 4 passive scalars with Schmidt numbers in the range 0.1 to 100 has been studied. The results show differences in mean concentration difference of up to 25%. As expected, that the major differences in scalar concentration occur where the velocity gradients are large, i.e. close to the nozzle and in the wall jet region.

INTRODUCTION

The understanding of turbulent mixing is important for many areas of application, such as: combustion, chemical and biochemical processes and medical applications. When simulating multi-species flows one often assumes equal diffusivities, since this simplifies the calculations and reduces the number of required equations. The assumption is then the diffusive effects will only be important for scales close to the Batchelor scale and hence the global effect will be negligible. However, this theory is developed in analogy with the Kolmogorov hypotheses and therefore only valid for very high Reynolds number, fully developed, isotropic turbulence. Unfortunately, in many practical applications this is not the case. One such application is the impinging jet which is used in many industrial applications where mixing is of importance such as enhancing the cooling and heating of surfaces, combustion and mixing processes in chemical and biochemical industry.

Several investigations of differential diffusion, both experimental and numerical, have been carried out in the past. Smith et al. (1995) studied, using Raman scattering, the non-reacting mixing of H_2 and CO_2 in a round air jet. They observed differences in average concentration for Reynolds numbers up to 1000. However, instantaneously the differential diffusion was detectable up to $Re = 64000$. Lately, the differential diffusion at high Schmidt numbers (1200 – 77000) far downstream in a in a low Reynolds number jet was studied by Saylor and Sreenivasan (1998). They found that the effects of different molecular diffusivities are active on scales much larger than the Batchelor scale.

The aim of this work is to, by using LES, investigate the effects of differences in molecular diffusivities in an impinging jet. The main focus is on the mixing in the wall jet region and the interaction with the coherent structures originating from the shear layer instabilities at the nozzle.

GOVERNING EQUATIONS

LES is based on spatial filtering of the equations of motion rather than time averaging used in traditional turbulence modelling. The space filtering of a function $f_i(x_1, x_2, x_3, t)$ is

defined as

$$\overline{f_i} = \int_{-\infty}^{\infty}\int_{-\infty}^{\infty}\int_{-\infty}^{\infty} G\, f_i dx_1' dx_2' dx_3' \qquad (1)$$

where $G(x_1 - x_1', x_2 - x_2', x_3 - x_3')$ is a filter function.

The space filtered non-dimesionalized equations for the conservation of mass and momentum for an incompressible Newtonian fluid can be written, using summation convention, as

$$\frac{\partial \overline{u_i}}{\partial x_i} = 0 \qquad (2)$$

$$\frac{\partial \overline{u_i}}{\partial t} + \overline{u_j}\frac{\partial \overline{u_i}}{\partial x_j} = -\frac{\partial \overline{p}}{\partial x_i} + \frac{1}{Re}\frac{\partial}{\partial x_j}\frac{\partial \overline{u_i}}{\partial x_j} - \frac{\partial \tau_{ij}}{\partial x_j} \qquad (3)$$

$$\tau_{ij} = \overline{u_i u_j} - \overline{u_i}\,\overline{u_j} \qquad (4)$$

where τ_{ij} is the Sub Grid Scale (SGS) stress tensor, which reflects the effect of the unresolved scales on the resolved scales. Since this tensor contains correlations of unfiltered velocities which are not explicitly known it has to be modelled. Usually the unresolved scales are modelled using the resolved quantities. However, as a first approximation one may take advantage of the properties of the numerical schemes. In the computational code used the convective terms are approximated by third order upwind finite differences. The truncation error from this approximation acts dissipatively, at least in an averaged sense, draining energy from the resolved scales. It has been reported by Gullbrand *et al.* (1998) that the energy flux caused by artificial (numerical) dissipation also can allow for some back scatter. Also, it has been shown by Olsson and Fuchs (1994) for a free jet that this term is of the same order and located in the same area as the SGS-term in a Smagorinsky model. However, it should be noted that for a given grid resolution the turbulent properties are improved by using explicit SGS models, e.g. Revstedt *et al.* (1998).

Passive Scalar Transport

For the concentration of an inert additive, c, the filtered transport equation can be written as

$$\frac{\partial \overline{c}}{\partial t} + \overline{u_j}\frac{\partial \overline{c}}{\partial x_j} = \frac{1}{Re\,Sc}\frac{\partial}{\partial x_j}\frac{\partial \overline{c}}{\partial x_j} - \frac{\partial \psi_j}{\partial x_j} \qquad (5)$$

where $Sc = \nu/D$ is the Schmidt number. The factor ψ_j in equation (5) is SGS mixing defined as:

$$\psi_j = \overline{u_j c} - \overline{u_j}\,\overline{c} \qquad (6)$$

The factor ψ_j has to be modelled since it too contains correlations between non-filtered variables. The same approach as for the SGS stress tensor has been applied, i.e. we use the discretisation truncation errors (numerical diffusion) to account for the SGS mixing.

NUMERICAL METHOD

The spatial discretisation of the governing equations is performed on a Cartesian staggered grid. The convective terms are discretised using the third order upwind scheme by Rai and Moin (1991). A fourth order central difference scheme was used for all other term (Olsson and Fuchs, 1998). Time integration is done by a four step explicit Runge-Kutta type scheme. A Poisson equation is solved for the pressure correction. To accelerate the solution of this equation a multi grid method is used.

The transport equation for concentration is solved only on the finest multi-grid level by using a converged velocity field. They are discretised using the same scheme as for the momentum equations. However, in order to avoid unphysical oscillations in the solution the spatial discretisation s switched to a lower order scheme if the exceeds the limits of maximum and minimum concentration.

Boundary conditions

No-slip conditions are set on all walls. At the jet nozzle both the velocity and the concentration was set to a "top-hat" profile. A random perturbation of 5 % of the average inlet velocity was superimposed on the nozzle velocity in all directions. At the outlet a Neumann condition corrected to ensure global mass conservation was applied.

The concentration of the inert additive was set to unity at the nozzle. On the wall and on the outlet boundaries the normal derivative of the concentration was set to zero.

COMPUTATIONAL SET-UP

The simulation were made on a semi confined impinging jet as shown in Figure 1. The impingement distance (D_{pw}) is varied between 2 and 6 nozzle diameters (D_0). The number of grid points for each impingement distance is presented in Table 1. To achieve higher grid resolution near the impingement wall and in the shear layers of the round jet we use analytical grid stretching functions also used by Olsson and Fuchs (1998). The advantage of using analytical functions is that exact expres-

sions for the derivatives used in the coordinate transformations can be calculated. Hence, one avoids introducing further numerical errors when evaluating the derivatives of the stretching.

Impingement distance	No. of nodes
$2.0D_0$	$96 \times 48 \times 96$
$4.0D_0$	$96 \times 96 \times 96$
$6.0D_0$	$96 \times 144 \times 96$

Table 1: Grid sizes

Four Schmidt numbers are considered, 0.1, 1.0, 10.0 and 100. This includes the range of Schmidt numbers one will find for the species in combustion of gaseous hydrocarbon fuels but also Schmidt numbers for larger molecules. Following Bilger and Dibble (1982) one can represent the difference in scalar transport using a mixture fraction (z). Due to the geometry and boundary conditions used here the this mixture fraction simplifies to:

$$z_{ij} = c_i - c_j \tag{7}$$

The cases considered in this work are listed in Table 2

Case	Sc_i	Sc_j	z_{ij}
1	0.1	1.0	z_{12}
2	1.0	10	z_{23}
3	10	100	z_{34}

Table 2: Schmidt number differences considered

The results will mainly be presented as time averaged concentration difference ($\tilde{z}_{ij}$), the rms. of concentration difference fluctuations ($z_{ij,rms}$) and the difference in rms. of concentration fluctuations ($\Delta c_{ij,rms} = c_{i,rms} - c_{j,rms}$).

RESULTS

The concentration differences occur mainly in two areas. Close to the nozzle the difference is very large due to the strong, thin shear layer. This initial difference is most probably responsible for the difference seen further down stream in the free jet region. However, the difference is smaller due to the increasing mixing by the developing turbulence. As the flow approaches the wall it is decelerated and redirected. In the proximity of the stagnation point one therefore again see differences due to the deceleration.

Consider the concentration difference along the developing round jet at $r/D = 0.5$, i.e. at the edge of the nozzle. As can be seen from Figure 2 there is a significant difference in mean concentration close to the nozzle. The difference is more pronounced for Case 1 however it is still clearly visible in Cases 2 and 3. This is an effect originating from the thin shear layer developing between the jet and the ambient fluid, i.e. low Schmidt number fluids diffuse faster over the shear layer. Further downstream the difference is decreased due to turbulent mixing and for Cases 2 and 3 it almost disappears. One can also see that there are no significant differences between the impingement distances.

As the jet approaches the wall it is redirected and a wall jet develops. Early stages of this development can be seen in Figure 3 depicting average concentration and concentration fluctuations for $Sc = 0.1$ and $D_{pw} = 4.0D_0$ at several distances from the centre line. Close to the centre line the concentration profiles are much affected by the free jet. As the flow exits the impingement zone (at about $r/D_0 = 1.2$ (Nossier, 1985)) the high concentration will be located closer to the wall and the maximum of concentration fluctuations will be at about 0.1 nozzle diameters from the wall. It should be noted that since Case 3 differs very little from Case 2, we only discuss Cases 1 and 2 below.

Taking a closer look at the wall region (Figures 4, 5 and 6) we see that the mean difference is is substantially larger for Case 1 than for the other cases. As the flow develops downstream the difference becomes slightly more pronounced. The same trend can be seen if we instead consider the difference in rms of concentration fluctuations. The fluctuations of concentration difference (z_{rms}) are somewhat higher than the Also, the maximum value of z_{rms} is much less affected by the Schmidt number, at least for the higher Schmidt numbers. One can also observe a decreasing difference in mean concentration and fluctuations with increasing impingement distance. This is expected since as the impingement distance is increased so is the turbulence level, which in turn will increase the turbulent mixing in the near wall region.

The probability density functions of z_{12} close to the wall ($r/D_0 = 0.03$) are shown in Figures 7, 8 and 9, for the three impingement distances, respectively. Considering the shortest impingement distance one sees that for the position closest to the jet centre line ($x/D_0 = 1.0$) it is evident that the distribution is very narrow and noticeable is that the peak value is not located at the average. Hence the distribution is somewhat skewed. As the jet develops the pdf will, as expected

be more Gaussian in shape. The same tendency, however not as pronounced, is seen for $D_{pw} = 4.0D_0$, whereas for $D_{pw} = 6.0D_0$ the skewed shape of the pdf is not visible. We believe that this behaviour is related to the fact that the coherent structures originating from the shear layer instabilities of the free jet will become less influential on the near wall mixing as the impingement distance is increased. However, further investigations are needed to confirm this.

In RANS calculations it is common practice to introduce a turbulent diffusion coefficient (D_t) in analogy with the eddy viscosity. From the LES data we estimate D_t in the wall normal direction from the following expression:

$$\widetilde{u'c'} = D_t \frac{\partial \tilde{u}}{\partial x} \tag{8}$$

where u' is the velocity fluctuation in the wall normal direction and '~' denotes time averaging. Here we estimate the turbulent Schmidt number ($Sc_t = \mu_t / D_t$) in the wall normal direction. It is plotted for two radial locations in Figure 10. Since we found no Schmidt number dependence in this parameter we only present the results for $Sc = 0.1$. Apart from some regions where the concentration gradient is very low, the turbulent Schmidt number has a value of about 0.1 in the wall jet.

CONCLUSIONS

Large Eddy Simulation of mixing a semiconfined impinging jet at Reynolds number 10000 was performed. The differences in scalar transport for several molecular Schmidt numbers have been studied. It is shown that differences are not detectable in an impinging jet at the Reynolds number at hand, even at relatively high Schmidt numbers.

The largest differences in mean concentration levels are found in two regions: in the shear layer close to the nozzle and in the wall jet close to the impingement wall. This is not surprising since in these regions the concentration gradients are high and the turbulence intensity is low. Hence, molecular diffusion plays an important role for the scalar transport normal to the flow. The differences close to the nozzle have a relatively large impact on the concentration levels downstream in the free jet. The concentration difference is decreased by turbulent mixing and as the flow reaches the wall it is substantially lower than at the nozzle. One therefore might therefore assume that the differences seen in the wall jet are only the remains of the initial differences at the nozzle. However, since an increasing difference is observed as the wall jet develops one can conclude that there is also some contributions to the differential diffusion in the wall jet flow.

ACKNOWLEDGEMENTS

This work was financially supported by the Swedish National Energy Administration (STEM) through the Fluid Mechanics programme.

REFERENCES

Bilger, R.W. and Dibble, R.W., 1982, "Differential diffusion effects in turbulent mixing", *Combust. Sci. Technol.*, Vol. 28, pp. 161-172.

Gullbrand, J., Bai, X-S. and Fuchs, L., 1998, "Large eddy simulation of turbulent reacting flows using Cartesian grid and boundary corrections", *AIAA paper*, 98-3317.

Nossier, N.S., 1985, "Impinging jets", *Encyclopedia of Fluid Mechanics*, N.P. Cheremisinoff, ed., Houston Gulf Publishers, Vol. 2, pp. 349-366.

Olsson, M. and Fuchs, L., 1994, "Significant terms in dynamic sgs-modeling", *Direct and Large Eddy Simulations I*, P.R. Voke, ed., Kluwer Academic Publishers.

Olsson, M. and Fuchs, L., 1998, "Large eddy simulations of a forced semiconfined circular impinging jet", *Phys. Fluids*, Vol. 10, pp. 476-486.

Rai, M.M. and Moin, P., 1991, "Direct simulations of turbulent flow using finite-difference schemes", *J. Comput. Phys.*, Vol. 96, No. 10.

Revstedt, J., Gullbrand, J., Guillard, F., Fuchs, F. and Trägårdh, C., 1998, "Large eddy simulations of mixing in an impinging jet", *Proc. of the 4th ECCOMAS Computational Fluid Dynamics Conference*, K.D. Papailiou et al., ed., John Wiley & Sons, pp. 1169-1174.

Saylor J.R. and Sreenivasan, K.R., 1998, "Differential diffusion in low Reynolds number water jets", *Phys. Fluids*, Vol. 10, pp. 1135-1146.

Smith, L.L., Dibble, R.W., Talbot, L., Barlow, R.S. and Carter, C.D., 1995, "Laser Raman scattering measurements of differential molecular diffusion in non-reacting turbulent jets of h_2/co_2 mixing with air", *Phys. Fluids*, Vol. 7, pp. 1455-1466.

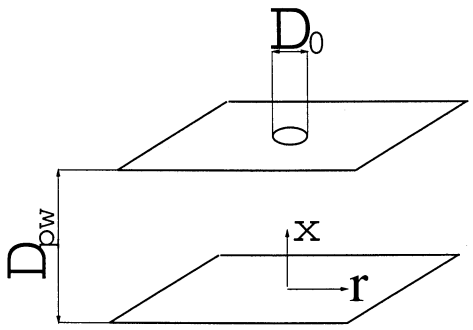

Figure 1: Simulation geometry and coordinate system

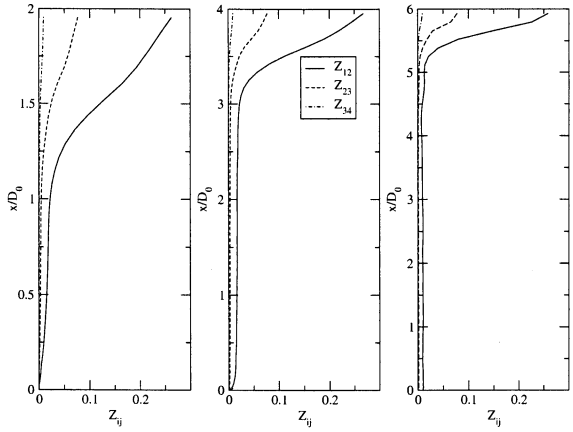

Figure 2: Mean concentration difference

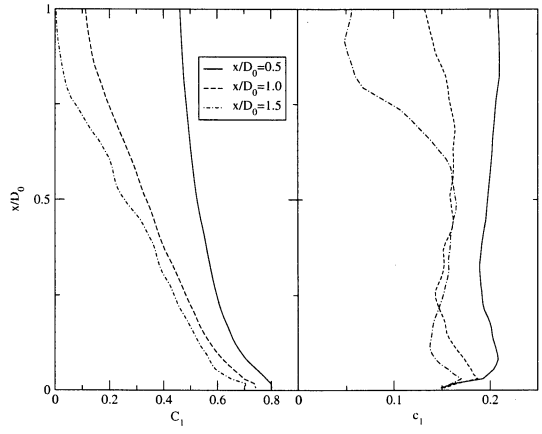

Figure 3: Mean concentration and rms of concentration fluctuations for $D_{pw} = 4.0D_0$

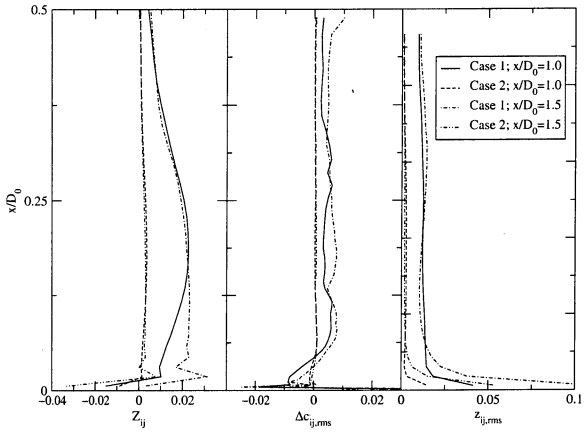

Figure 4: Mean concentration difference (left), difference in rms of concentration fluctuations (middle) and rms of concentration difference fluctuations (right) for $D_{pw} = 2.0D_0$

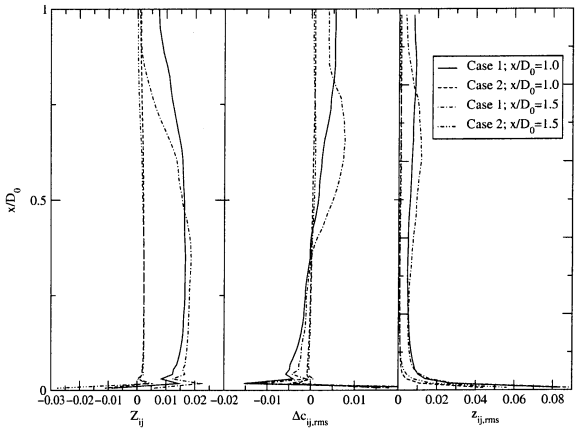

Figure 5: Mean concentration difference (left), difference in rms of concentration fluctuations (middle) and rms of concentration difference fluctuations (right) for $D_{pw} = 4.0D_0$

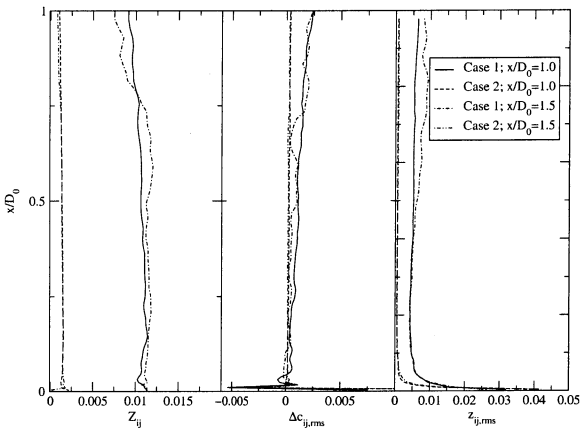

Figure 6: Mean concentration difference (left), difference in rms of concentration fluctuations (middle) and rms of concentration difference fluctuations (right) for $D_{pw} = 6.0D_0$

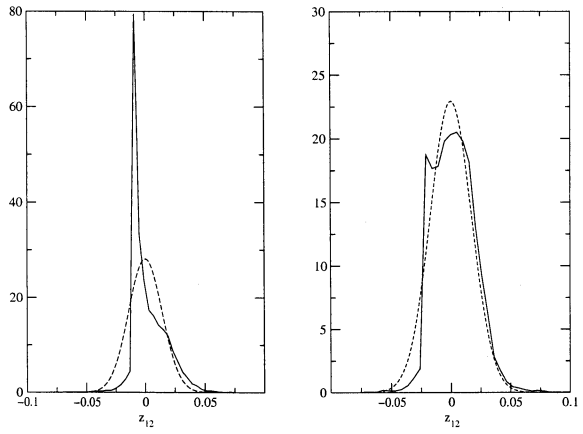

Figure 7: Probability density function for z_{12} at $x = 1.0D_0$ (left) and $x = 1.5D_0$ (right) for $D_{pw} = 2.0D_0$

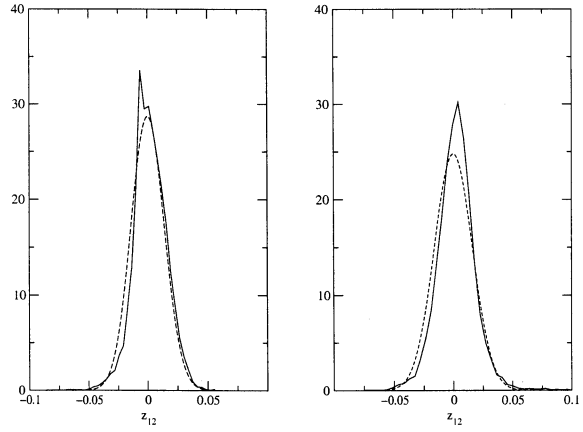

Figure 8: Probability density function for z_{12} at $x = 1.0D_0$ (left) and $x = 1.5D_0$ (right) for $D_{pw} = 4.0D_0$

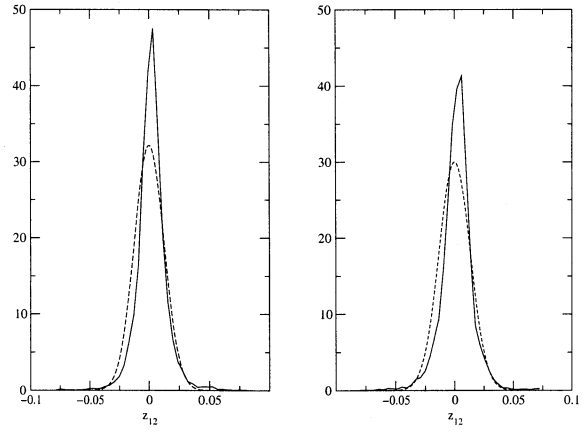

Figure 9: Probability density function for z_{12} at $x = 1.0D_0$ (left) and $x = 1.5D_0$ (right) for $D_{pw} = 6.0D_0$

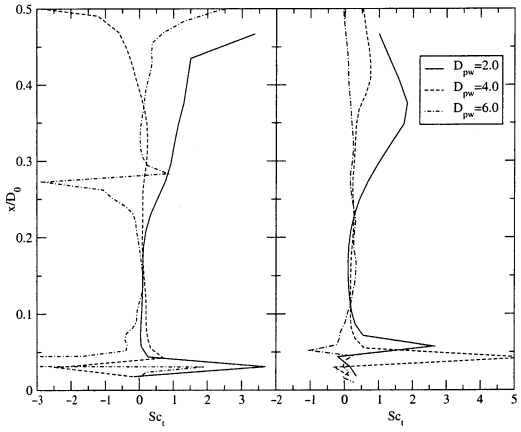

Figure 10: Estimation of the turbulent Schmidt number at $x = 1.0D_0$ (left) and $x = 1.5D_0$